# Cooled pads with bioinspired gyroid lattice for tilting pad journal bearings: Experimental validation of numerical model for heat transfer

Ludovico Dassi [*], Steven Chatterton, Paolo Parenti, Andrea Vania, Bianca Maria Colosimo, Paolo Pennacchi

*Department of Mechanical Engineering, Politecnico di Milano, Via La Masa 1, 20156 Milan, Italy*

## ARTICLE INFO

## ABSTRACT

Hydrodynamic journal bearings are essential components for industrial rotating machineries. Continuously growing specific power allows more compact and efficient machines to be obtained, by reducing the environmental footprint of production plants. The aim of this work is to provide a new design of an innovative pad for Tilting Pad Journal Bearings (TPJBs) with an embedded cooling circuit, able to limit the oil film temperature. As a result, specific load can be increased leading to a possible downsizing of the bearing and reduction of lubricant quantity. The heat exchange in the cooling circuit of the pad has been enhanced using bioinspired gyroid lattice. The thermo-mechanical study of the pad has been performed with both numerical and experimental analysis. The resulting thermal and mechanical performances have been calculated and discussed. The tested components have been manufactured in stainless steel by using a metal 3D printing technology, based on polymer-metal feedstock extrusion. A performance analysis is conducted to catch differences between the nominal and the printed geometry. The prototype is able to dissipate the generated heat with a higher efficiency, and the pressure drop inside the cooling circuit can be estimated with the numerical model here proposed.

## 1. Introduction

Hydrodynamic journal bearings are standard equipment for supporting shaft lines in turbomachines. This technology provides many advantages such as higher load capacity, lower frictional losses and lower maintenance cost than rolling element bearings. Moreover, the well-known instability issue of cylindrical hydrodynamic bearings can be faced by adopting a tilting pad layout to make the system stable even at high rotational speeds.

Nowadays, the recent machine design and energy trends require an increase of specific power in production plans and fast start up procedures. This approach increases the efficiency of the machines but it requires a more demanding design of the components, including the bearings [1]. Vibrations due to non-linear behavior can induce instability issues, as discussed by Kim et al. in [2]. In particular, the operating range of tilting pad journal bearings is strongly influenced by the thermal distribution of the sliding surfaces, which results in a thermal pad deformation and in a distorted pressure distribution, as studied by Fillon in [3]. Then, excessive heating of the component, due to the frictional losses in the oil film wedge, is the main limitation increasing the load

capacity, reducing the coating wear and failures occurrences. In particular, fatigue is an important issue for the sliding surfaces of the bearing, as studied by Dong et al. about cavitation phenomena [4] and Yang et al. about the fluttering condition of the upper pads [5]. In the last few years, many research activities have tried to implement active temperature control by proposing different layout solutions. For example the oil mass flow from the jacking pump circuit can be tuned in order to modify the dynamic characteristics of the bearing [6,7]. Moreover, new design solutions, like the leading edge groove, have increased the cooling capacities and reduced the oil consumption. This layout has been deeply investigated by many authors, such as Hagemann et al. [8] and Abdollahi et al. [9]. The reduction of oil temperature is accomplished by increasing the turbulence intensity [10] and by implementing an active control on the delivered oil quantity [11]. Schüler et al. [12] further improve the oil cooling by exploiting the effect of turbulence generated by eddy grooves, or Yang et al. in [13] implement a power loss reduction technique by favouring oil cavitation. By inserting a pocket and step feature in the pads, it is possible to reduce the power losses by up to 27 % with beneficial effects on maximum speed and surface temperature.

---

The internal cooling of pads, by using a dedicated circuit, is a promising arrangement to properly cool down pads. Starting from 2014, Najar and Harmain [14] have proposed and quantified the advantages of using a water-cooling circuit with different channel shapes (M-shaped or bifurcated path) for a thrust bearing pad, studying and updating the geometry in another paper [15]. In this last manuscript the theoretical analysis is carried out by a numerical model to predict the temperature distribution into the pad. The most relevant outcome is that the cooling circuit can remove up to 30 % of the thermal power generated by the oil friction.

To overcome the production complexities of the cooling circuit, Additive Manufacturing (AM) technologies can be used. Chatterton et al. in [16] address this topic, by considering a journal bearing and a cooled pad with an M-shaped channel. Firstly, they created an advanced Thermo-Elastic-Hydro-Dynamic model to compare the performances of different channel cross sections and then they made a functional prototype of the component [17]. The best results are obtained by using a 6-square-multichannel arrangement as cross section of the cooling circuit. The results show that the average surface temperature is significantly reduced with respect to the same pad without an internal cooling circuit. The numerical model has also been validated by an experimental campaign.

An innovative way to further improve the dissipated heat from the cooling circuit is to increase the exchanging area and to sustain vorticity in the coolant. The evolution of metal 3D printing technologies allows increased geometrical freedom, therefore complex internal structures can be shaped inside the pad to accomplish this task. For instance, gyroid lattice is a bioinspired innovative geometry with relevant heat exchange properties, as discussed by Kaur et al. in [18]. As reported by in Li et al. in [19], gyroid lattice has been discovered by the NASA physicist Alan Schoen in 1970 s, by studying the nanoscale biological microstructures of C. Ruby species butterflies by using a Scanning Electron Microscope (SEM). It has been found that wing microstructure is organized in complex and hierarchical structures on different length scales to realize different functions and to adapt to natural environments. The main surfaces are covered by interconnected ridges and ribs, providing mechanical stability, and serving as interference reflectors to dump external forced vibrations.

The basic idea of this paper is to take advantage of metal 3D printing technology to design complex geometries which can enhance the heat transfer performances by means of an increased heat transfer contact area and compactness [20]. As a result, heat exchangers of new generation, called Printed Circuit Heat Exchangers (PCHE), can be designed and manufactured. Thanks to their small overall dimensions, lightweight structures, and improved high heat transfer efficiency they can find many innovative application fields, such as CO2 supercritical Rankine cycles [21]. Among the available lattice structures, that can be found in the literature, only gyroid lattices have been investigated in this paper. The main advantages of such lattices are the increased exchanging surfaces, the possible onset of turbulent condition and the continuous rounded shape without sharp edges which is beneficial for the mechanical resistance. Thus, the channel can contribute supporting the load.

The aim of this manuscript is to provide a preliminary thermo-mechanical design of a cooled pad with a conformal cooling circuit based on gyroid lattice. Both oil ISOVG68 and water are considered as coolant fluids, while the pad is made of stainless steel SS316L with a white metal SbSn8Cu4 lining. Numerical simulations were performed for a proper selection of the lattice design parameters. The structural behavior was estimated by *Finite Element Modelling* (FEM) analysis while the heat exchange and internal fluid dynamics of the coolant by *Computational Fluid Dynamics* (CFD). A discussion on the simplification hypothesis and modelling schemes of the complex internal geometry are included. Pad geometry design is addressed by taking into account the requirements of the functional component, as well as the technological constraints given by the adopted AM process. After building the prototypes, experimental flushing has been performed to catch differences between the printed geometry and the nominal one considered in the fluid-dynamic model.

## 2. Gyroid lattice structures

### 2.1. Analytical definition

From the analytical point of view, the gyroid is formalized as a Triple Period Minimal Surface (TPMS) geometry [22]. The surface is defined as minimal, when it locally minimizes its surface energy given a certain boundary. As a result, it has smooth curvatures with no edges or corners. TPMS geometries without self-intersections divide the domain into two disjoint and intertwining domains, which are simultaneously continuous. The level-set approximation technique is used to obtain TPMS lattices, which have cubic symmetry and they are periodic in the three-dimensional space. The fundamental equation of minimal surface for gyroid is reported here:

$$\phi(x, y, z) = \cos(x)\sin(y) + \cos(y)\sin(z) + \cos(z)\sin(x) = 0 \tag{1}$$

where $x, y, z$ are cartesian coordinates.

Once the minimal surface is defined, there are two possible ways to create gyroid structures. The first one relies on the surface thickening and brings to sheet based TPMS structures. The surfaces facing towards the individual domains are offset in two directions perpendicular to the surface, creating a solid wall with a homogeneous thickness (Fig. 1a). The second way is obtained by solidifying one of the two volumes defined by the minimal surface, yielding to a skeletal based TPMS structure (Fig. 1b).

The relevant parameters which have to be set to fully define the gyroid lattice shape are: the lattice type (sheet or skeletal), the unit cell length (edge of the minimum repeatable cell), the relative density (percentage of solid volume in an elementary cube) and the external lattice dimensions (obtained by repetition in space of the minimum cell).

### 2.2. Heat exchange properties

The gyroid lattice can guarantee relevant performances for TPJB applications. According to Li et al. studies [19], also confirmed by several other authors like Koneri et al. [23] and Zhang et al. [24], gyroid lattice figures out the best heat transfer rate with respect to the other open cell periodic lattices. The authors considered a simple cylindrical pipe used as a representative section of a heat exchanger, water is used as coolant and the temperature of the outer shell is imposed. The pipe is then filled with a selection of the more promising lattices (i.e. gyroid, Star Kogeme and Cubic body centered). The comparison is conducted by considering the pressure drop needed for the circulation of a specified coolant flow rate and the heat transfer rate between the coolant and the outer shell, as shown in Fig. 2.

From the results, gyroid lattice figures out the highest values of both the two variables with respect to the other lattices. The heat exchange can be increased of 50–60 % with a higher pressure drop + 500 % as drawback. The Overall Enhancement Factor (OEF) is a suitable indicator to effectively quantify the increase of heat exchange with respect to the pressure increase [23]. The definition of the OEF is reported in the following expression:

$$OEF = \frac{Q/Q_0}{\Delta P/\Delta P_0} \tag{2}$$

where $Q$ and $\Delta P$ are the heat exchange and the pressure drop of the considered lattice while $Q_0$ and $\Delta P_0$ are the same quantities referred to a plain cylindrical pipe. According to the authors, the OEF of the gyroid lattice is 3 times higher than other lattices.

For practical design criteria, since the heat transfer power is some order of magnitude higher than the required hydraulic power, it is a
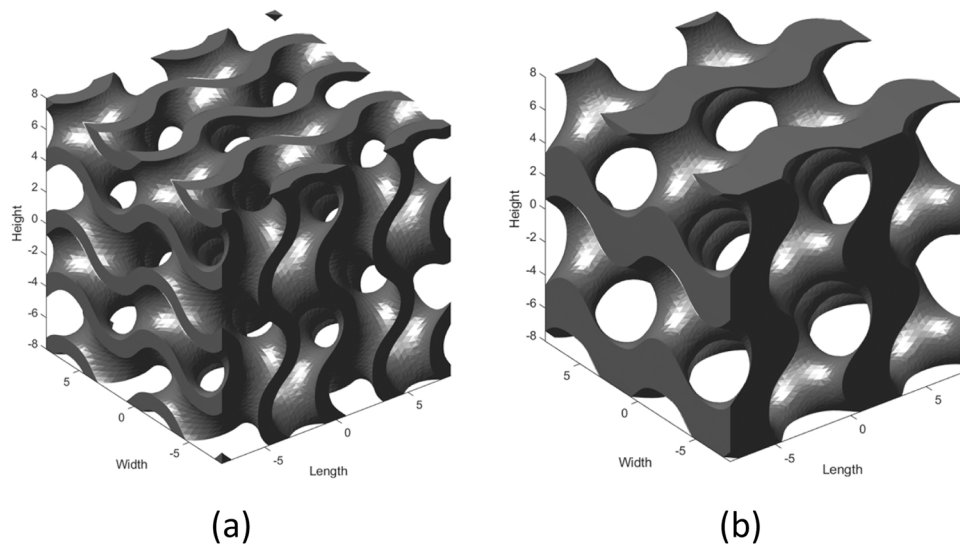
**Fig. 1.** Gyroid lattice 3D models: (a) sheet based, (b) skeletal based.
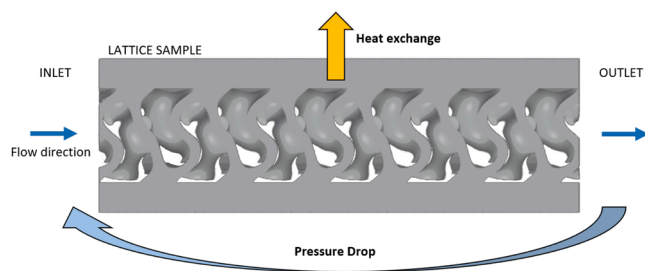


**Fig. 2.** Schematic representation of the thermal-fluid quantities of interest.

common practice to simply limit the pressure drop to a desired value, convenient for the application. So that, the increased heat exchange becomes the most relevant quantity to be maximized.

### 2.3. Mechanical properties

The gyroid lattice features relevant mechanical properties for its lightweight. Al-Ketan et al. [25] intensively studied the mechanical resistance and stiffness of several lattices with respect to the bulk material, under the hypothesis of periodic structure and linear deformations. By considering the dominant deformation modes of the unit cell, the authors justified the higher structural efficiency of the gyroid lattice by noticing that tensional axial stresses are promoted inside the thin walls, while other lattices (i.e. diamond and octet truss) are dominated by bending modes. This fact increases the gyroid lattice stiffness and, consequently, the relative Young modulus generally reaches 5 % with respect to the bulk material and the ultimate strength around 10 %.

### 2.4. Printability

Due to the high complexity of pad internal geometry, the most suitable technology for the production is metal AM, a technology that allows producing 3D functional prototypes in metal with a near-net-shape output, as presented in [26]. In particular, material extrusion Metal 3D printing technology, i.e. the Bound Metal Deposition (BMD) system, is chosen for its advantages. The production route is composed by three main steps which are: the printing of the feedstock at low temperature (around 180 °C), debinding from polymeric binder and sintering in an electric furnace (around 1360 °C for the adopted stainless steel SS316L). One of the key advantages is that, after printing, there is

no resulting powder to be flushed away from internal cavities, which may be a difficult operation for a complex shaped channel. Moreover, this technology is flexible as it is successful in handling a wide range of materials, including copper, which is a promising pad development. Furthermore, this technological solution reaches high dimensional-geometrical precision [27], reducing printing defects and porosity issues, which are detrimental for the mechanical properties of the pad.

## 3. Design of pad geometry

### 3.1. Preliminary design choices

The considered bearing is a five-pad TPJB with nominal shaft diameter of 100 mm. The most relevant data of the bearing are listed in Table 1. The geometry layout is a rocker-back pivot in load-on-pad configuration (LOP), as shown in Fig. 3a. The pressure and the temperature distributions are calculated by means of a bearing model, fully described by the same authors in some previous articles, such as [28] and [29]. The resulting plots are shown in Figs. 3b-3c and they are used as input for the current analysis. For the sake of simplicity, the temperature field is reduced to a uniform distribution equal to the mean value (60 °C).

The journal bearing is composed of five flooded lubricated pads, and only the bottom one, the more loaded, is assumed to be internally cooled, whereas the optimal solution is represented by all cooled pads. The baseline cooling arrangement is composed of an M-shaped circuit characterized by 6-squared channels cross section, as shown in Fig. 4a. The baseline design is the same already investigated by the same authors

**Table 1**
Bearing data.

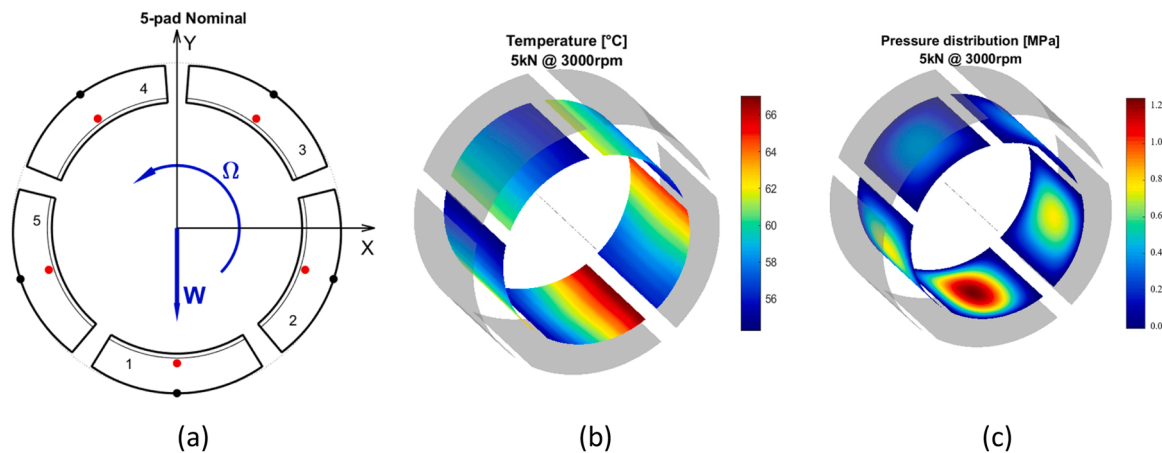| Property | Value |
| --- | --- |
| Shaft diameter [mm] | 100 |
| Pad outer radius [mm] | 59.60 |
| Pad length [mm] | 70 |
| Assembled clearance [μm] | 60 |
| Machined clearance [μm] | 130 |
| Pad span angle | 60° |
| Total pad thickness [mm] | 16 |
| Lubricant | Oil ISOVG68 |
| Oil flow rate [L/min] | 2 |
| Load [KN] | 5 |
| Speed [rpm] | 3000 |

**Fig. 3.** (a) Bearing assembly sketch, (b) temperature distribution and (c) pressure distribution.
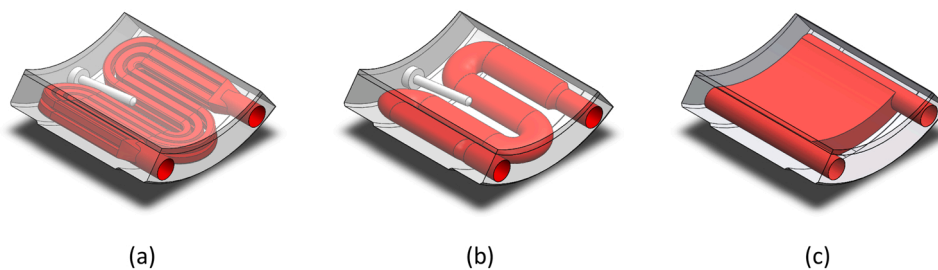


**Fig. 4.** (a) Baseline solution, (b) M-shape-path filled with gyroid, (c) diffused gyroid lattice.

in [16] and manufactured by Selective Laser Melting (SLM) process. The outer dimensions of the pad are kept constant and only the internal cooling circuit is changed in the new proposed solution. For a successful design, both mechanical and thermal aspects must be considered. On the one hand, the gyroid lattice should increase the maximum heat exchange, but on the other hand it should not negatively impact on the actual mechanical stiffness of the 6-channels pad. First of all, two possible new designs for the internal layout have been investigated with respect to the baseline. The first design is to keep the M-shaped channel and fill it with gyroid lattice (Fig. 4b), choosing accurately the cross-sectional area and the lattice parameters to balance the performances. The second one is a cross flow heat exchanger that can be created with two parallel channels and a diffused gyroid lattice in the central portion of the pad internal volume, as shown in Fig. 4c.

The last layout has been disregarded due to its lack in mechanical stiffness, while being interesting for the larger internal volume and the relevantly improved thermal properties. From the literature data on TPMS lattices [30], the maximum compression stiffness is, in fact, 5 % of the bulk material and it is considered not enough for pad application. The resulting compliances would affect the oil film wedge and shaft line dynamics with unpredictable effects, so M-shaped layout has been chosen in this study.

### 3.2. Estimation of bearing improvement

From the mentioned literature, pad internal cooling is a promising solution and it can extract up to 30 % of the heat generated by oil friction in the bearing. Moreover, gyroid lattice is able to further boost the heat exchange in cooling channel by enhancing fluid turbulence regime. The development of a fully TEHD model of the cooled pad is onerous but a simplified analysis is here proposed to figure out the important advantages of the gyroid cooling solution. By considering as example, the 5-pads bearing described by the same authors in [28] and [29] with the data here listed in Table 1, the calculations are repeated. Oil film

Reynolds equations are solved by adding an heat sink term to mimic the presence of the internal cooling channel only in the bottom pad, the most loaded one. The analysis is performed by expressing the heat dissipation as a percentage of the viscous heat production. A flow rate of 6 L/min and inlet temperature of 40 °C is assumed in the analysis. The reference condition is given by the case with null heat removal in Fig. 3b. The reduction of oil film temperature by considering the case of heat removal from the pad #1 only is shown in Fig. 5a. The maximum cooling effect occurs in the pad #1, while the other pads are affected in a gradually decreasing manner. The last pad #5 is not influenced by the heat removal on the bottom pad. The reduction of the temperature leads also to a positive increase of the bearing performance in terms of minimum oil film thickness, as shown in Fig. 5b. The estimated power loss in the bearing is almost constant.

Moreover, the reduction of the maximum temperature in the bearing allows to downsize the bearing dimensions or to increase the bearing load capacity. For example, by considering the same bearing dimensions, assuming a heat removal of 30 % from pad #1 only and setting the maximum temperature on pad #1 to the value of 67 °C obtained in the reference condition, the load can be increased of approximately 80 % or the oil flowrate reduced of 30 %. In the nominal bearing, without heat removal from pads, the increase of 80 % of the load corresponds to an increase of the maximum temperature on pad #1 from the nominal condition of 67 °C to approximately 72 °C, whereas a reduction of 30 % of the oil flowrate corresponds to an increase of the maximum temperature on pad #1 from the nominal condition of 67 °C to approximately 71 °C.

### 3.3. Internal lattice choice

To facilitate the comparison with the baseline layout, the net cross-sectional area available to the fluid, has been kept equal to the original amount, i.e. 50 mm². By considering an internal filling with lattice geometries and choosing a percentual available area of 67 %, the
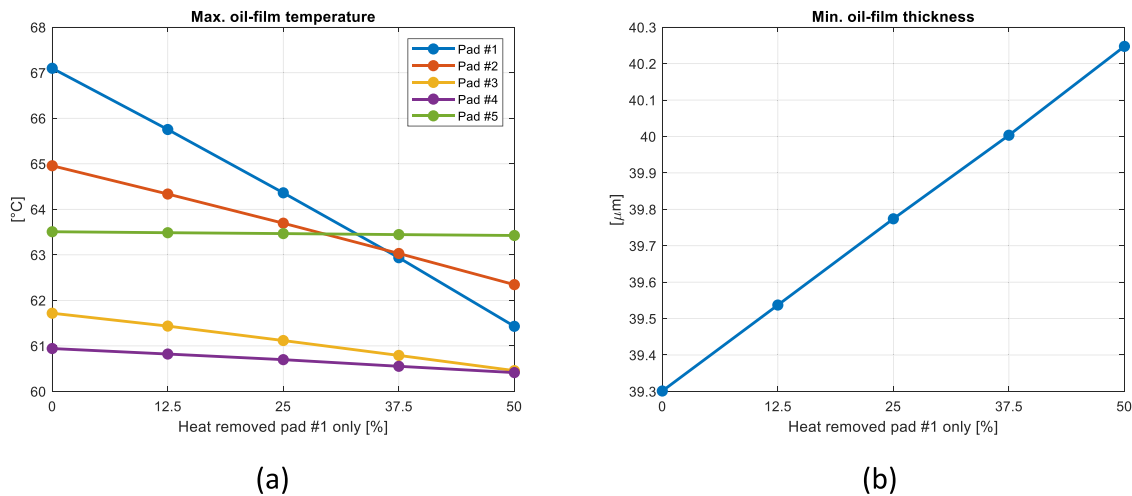
**Fig. 5.** Improvement of performances for gyroid cooled bearing: Maximum oil film temperature (a), minimum oil film thickness (b).

channel total section area is calculated as 75 mm². An elliptical duct (8 mm × 12 mm vertical and horizontal main axis respectively) guarantees the area and correctly fits with pad dimensions; in addition, round edges avoid stress intensification, and assure better printability of the component.

In this regard, cell length is chosen to be 8 mm to guarantee the printability, while the lattice type is arbitrary and the relative density should range in the interval 20–50 %. Since the scientific literature is still incomplete in comparing the performances of different gyroid lattices geometries, a preliminary study is here performed to define the set of parameters with mechanical a thermo-fluid dynamics performance best fitting to the given application.

The fluid-dynamics performances of the lattice are here investigated carrying out both numerical and experimental tests. Simple cylindrical samples, i.e. "tubes", manufactured in stainless steel SS316L and filled with different gyroid lattices, are considered to mimic the functioning of the final pad, whilst simplifying the numerical and experimental investigations. In particular, a thermo-fluid dynamics analysis is performed to find the best trade off on performances (pressure drop and heat exchange) for pad application. The considered tubes are 50 mm long (1/4 of the total length of the pad cooling circuit), while the cross-sectional area is equivalent to the one of the baseline pad geometry. The analysis has been performed to directly match the different lattice geometries and to study the effects of the parameters settings (cell length, relative density, working fluid) on the fluid dynamic properties of interest. Therefore, six lattice layouts are selected for the analysis by changing the lattice type and the relative density; namely densities 35, 45 % for sheet structure and densities 12, 25, 35, 45 % for solid structure as reported in Table 2. Relevant dimensions for used lattice are: cell length= 8 mm and wall thickness= 1 mm. Sheet lattices with lower relative density are not considered because they face relevant printing problems with BMD technology. The choice of dimensions for cylindrical tubes should take into consideration the printing limits of Additive manufacturing. The tube inner diameter is 10 mm and a length is 50 mm. The proposed geometry can be scaled or repeated in space without relevant constraints, except for the minimum wall thickness which should be greater than 1 mm for the used BMD technology.

The types of the boundary conditions have been chosen similarly to

the existing ones in the literature [23] while the values are chosen for the application, in particular a flow rate of 6 L/min and inlet temperature of 40 °C are assigned for the coolant while temperature of the outer wall of the tube is imposed to 60 °C. Both oil ISOVG68 and water are analysed. Mesh sensitivity analysis and experimental validation are performed to validate the numerical model on the pressure drop with errors lower than 5 %. An example of the computed pressure and temperature fields from the numerical analysis are shown in Fig. 6a and Fig. 6b while a printed tube is shown in Fig. 6c.

The main goal of this analysis is to increase as much as possible the heat transfer between the outer tube shell and the flowing coolant, while taking into account the increase of back pressure for the coolant, by considering the OEF index. From the results, sheet lattice has a higher heat exchange performance compared to the solid one (Fig. 7a) probably because of the more finned lattice structure, so it is preferred. Then the sheet lattice with RD= 35 % figures out a higher OEF with respect to RD= 45 % (Fig. 7b). The OEF factor is calculated according to Eq. 2, by considering the heat exchange and counterpressure values calculated for each lattice. A higher OEF is favorable because it means a lower pressure drop for the fluid. These considerations are valid both for oil and water as coolant but water figures out a three times higher heat exchange values. The full analysis on the tubes samples not reported here for the sake of brevity. Finally, gyroid lattice with sheet layout and relative density RD= 35 %, named "sheet 35 %" in the following, is chosen for the pad application.

### 3.4. Pad design for a successful manufacturing

The manufacturing with the AM process requires geometrical corrections to provide the successful production of the pads. Common rules for AM design have been considered, in terms of printing tolerances, maximum overhang angles and supported structures, part sintering stability, maximum aspect ratio and filament stringing issue. Then, a metal stock of 1 mm is added over all surfaces for enabling subsequent mechanical finishing operations by milling process. The addition of local lattice piercings and venting holes, shown in Fig. 8, are useful to speed up the production time during the debinding phase. Moreover, lattice piercings help to balance the pressure between the two fluid domains of gyroid lattice, in particular near channels curves. An example of the unbalanced pressure field is shown in Fig. 15, where piercings are intentionally not present.

The pad is printed in stainless steel SS316L, with vertical orientation in two specimens by varying the printing orientation angle. Delamination issues arise with horizontal layering while a 20° pad tilting avoids this issue. It is also relevant to consider that the surface roughness
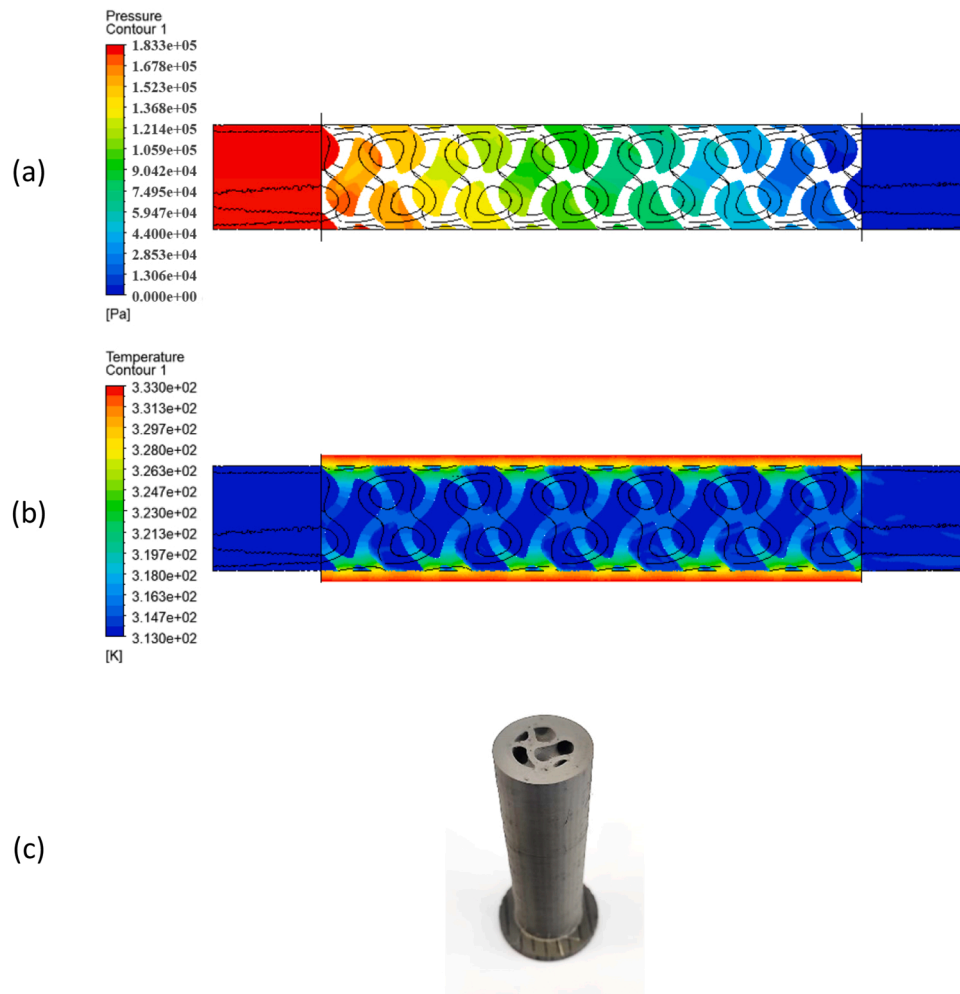
**Table 2**
Types of gyroid lattices for filling of tubes.

| Type \ Density | 15% | 25% | 35% | 45% |
| --- | --- | --- | --- | --- |
| Sheet | ✗ | ✗ | ✓ | ✓ |
| Solid | ✓ | ✓ | ✓ | ✓ |

**Fig. 6.** Analysis of tube filled with "sheet 35 %" lattice: numerical results of pressure (a) and temperature (b) fields; functional prototype "sheet 35 %" tube (c) for preliminary study.
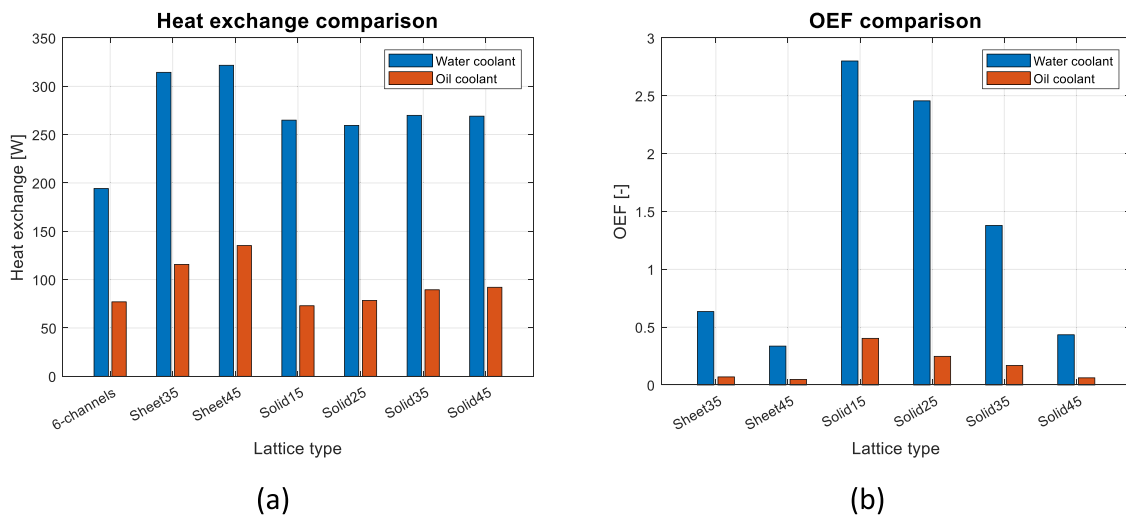


**Fig. 7.** Comparative analysis on gyroid lattices with flow rate 6 L/min:Maximum exchangeable heat (a), Overall Enhancement Factor (b).

changes, depending on the layering orientation. The pad printed with vertical orientation, labelled as pad #1, has a surface roughness of Ra= 16 μm while the pad printed with an orientation of 20°, labelled as pad #2, has a roughness of Ra= 22 μm. This aspect is properly measured with an optical 3D microscope (Brucker Alicona G4) since it will affect the internal fluid dynamics of the coolant. Finally, only pad #2 is coated with Babbitt (white metal), and it is mechanically finished in all the surfaces making it ready for the final application. The prototype of pad
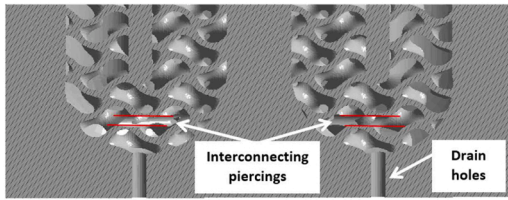
**Fig. 8.** Details of internal channel design: lattice piercings and drain holes.

**Table 3**
Materials mechanical properties.

|  | Base part | Lining |
|---|---|---|
| Material | SS316L | SnSb8Cu4 |
| Mass density [kg/m$^3$] | 8030 | 7300 |
| Young modulus [GPa] | 200 | 53 |
| Poisson ratio | 0.3 | 0.35 |
| Compressive Yield Strength [MPa] | 300 | 89 |
| Tensile Yield Strength [MPa] | 300 | 80 |

#2 is shown in Figs. 9a-b, while pad #1 is rejected due to leakage and delamination issues. Actually, pad #1 has been only used for comparative analysis on pressure drop. A visual inspection of the internal channel for the pad #2 is shown in Fig. 9c.

## 4. Pad deformation

### 4.1. FEM simulation setup

The pad is, at first, a structural element of the bearing, therefore a finite elements static structural analysis has been performed to calculate static deformations of "sheet 35 %" lattice and other type of lattices. The purpose of this analysis is to compare the static deformation of the component depending on the internal lattice type, where the effect of temperature is here neglected. A FE model of the pad is generated considering the complex lattice geometry adopted and Babbitt alloy coating on the top surface. The material properties are listed in Table 3. Stainless steel SS316L and standard Babbitt alloy SnSb8Cu4 have been assumed for the base part and the lining of the pad, respectively.

The FEM simulations have been performed with the same external loading conditions in [29]. The pressure distribution to be applied to the pad surface is shown in Fig. 3c. Geometry is clamped in the pivot region along an artificial strip surface; this allows simplifying the case, avoiding the implementation of a contact model, even if this boundary condition causes some localized stress intensification in the bottom surface, which is not of interest for this part of the proposed study. To simplify the analysis, the effect of thermal expansion is neglected at this phase and only the effect of the static load is considered. So, no temperature effects have been considered in this analysis. A tetrahedral mesh is used to adapt cells to complicate lattice geometry and mesh sensitivity analysis is performed.

### 4.2. FEM results analysis

The computed Von Mises stress and the pad deformation for the lattice "sheet 35 %" are shown in Fig. 10. The proposed solution guarantees no stress intensification inside the lattice domain and low absolute values of Von Mises stress (40 MPa). This is an important aspect to prevent cracking formation between the printed layers.
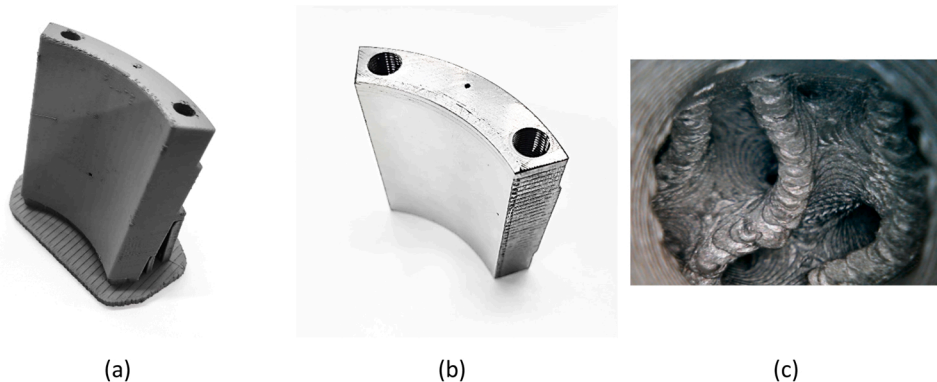
The maximum deformations of the pad for different lattice structures, as well as their relative deformation with respect to the baseline, are listed in Table 4. Both the lattice type (sheet or solid) and the relative density (15–45 %) are varied. The deformations have been estimated as the maximum vertical deformation of the pad geometry, located in the corner tip of the sliding surface when the nominal load is applied. The stiffness value is not calculated because in TPJB the overall stiffness coefficient of the bearing is mostly given by the oil film, which highly depends on the oil wedge shape. As confirmed by Fillon in [3], pad deformations due to mechanical and thermal effects are more important than the sole pad stiffness.

Looking at the results, "sheet 35 %" lattice has 11 % less deformation than the baseline solution, so gyroid lattice is more beneficial on the load carrying capacity than squared channels. The best result can be obtained with a "sheet 45 %" lattice, even if this lattice structure shows an excessively high pressure drop for the cooling circuit, so it has not been chosen for the prototypes.

## 5. CFD thermo-fluid-dynamic analysis

### 5.1. CFD simulation setup

A numerical model is used to study the thermal diffusion phenomenon of the pad and internal fluid dynamics. For a generic material element, thermal diffusion is governed by the Fourier-Biot relation, as follows:

$$K \cdot \nabla^2 T = \rho \cdot C \cdot \frac{dT}{dt} - \dot{g} \qquad (3)$$

where $K$ is the thermal conductivity coefficient, $T$ is the temperature, $\rho$ is the material mass density, $C$ is the specific thermal capacity and $\dot{g}$ is the source coefficient. This model is valid both in solid and fluid domains, where also advection term is present in the latter one.

For the pad case study, Navier-Stokes equations are solved to predict the fluid dynamics regime under hypothesis of steady state condition, viscous and incompressible fluid. To consider the turbulence effects, a 2-equations $k - \omega$ SST (Shear Stress Transport) model has been used. Actually, it is the most common choice for complex flow calculations, and it is presently considered the standard choice for RANS (Reynolds
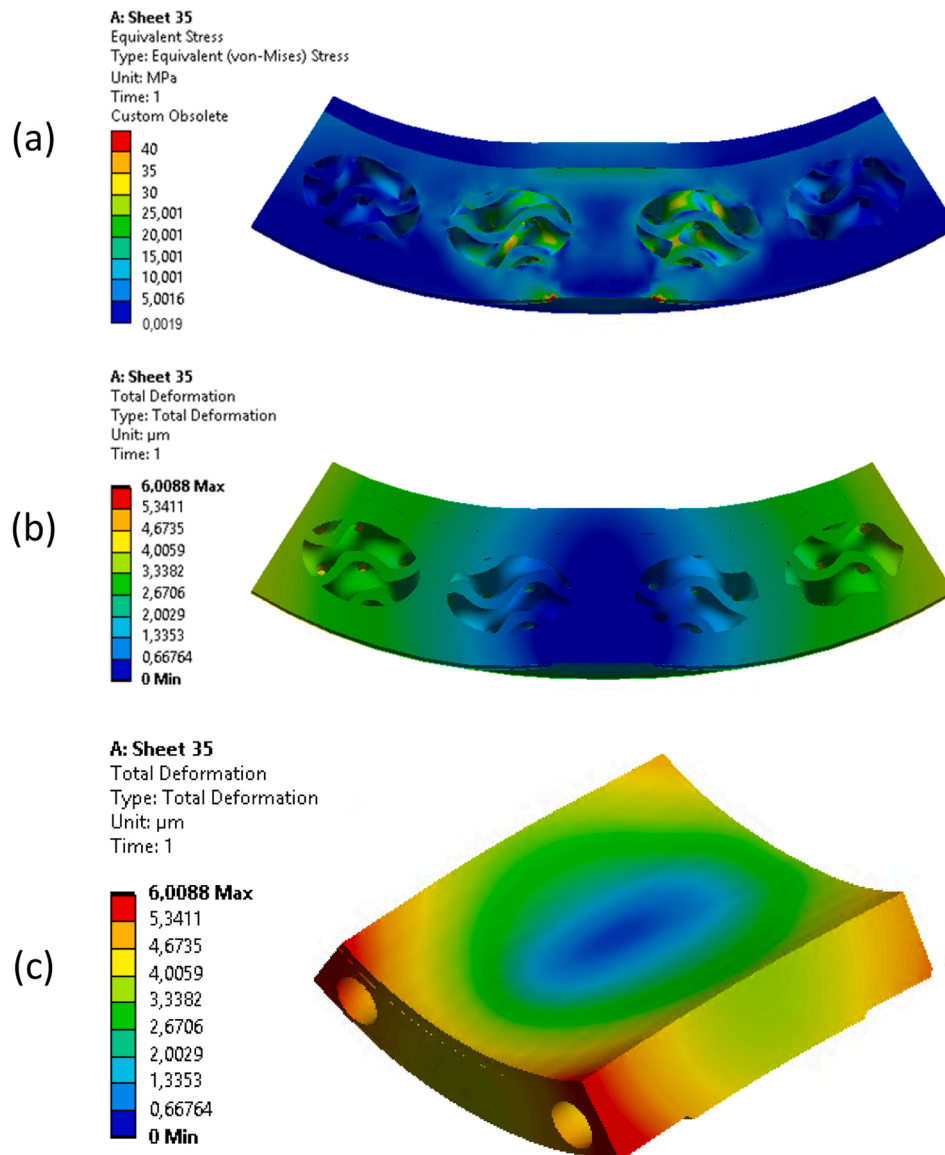


**Fig. 9.** Functional prototype of pad #2 as printed (a) and coated and milled (b), inspection of internal channels (c).

**Fig. 10.** Results of static FEM analysis of pad with "sheet 35 %" gyroid lattice infill under nominal load: (a) Von Mises stress, (b, c) total deformation.

**Table 4**
Static deformation for different pad internal infill lattices.

| Internal Layout | Maximum deformation [μm] | Deformation difference [%] |
|---|---|---|
| 6-channels | 6.77 | - |
| Sheet 35 % | 6.00 | -11.3 % |
| Sheet 45 % | 4.11 | -39.2 % |
| Solid 15 % | 7.70 | +13.7 % |
| Solid 25 % | 6.85 | +1.2 % |
| Solid 35 % | 6.21 | -8.3 % |
| Solid 45 % | 4.31 | -36.4 % |

Average Navier-Stokes equations) calculations in this field of application. The $K-\omega$ *SST* model fully solves boundary layer development under the hypothesis of no slip condition and it requires the check of the *adimensional momentum thickness* $(y+)$ value at the walls. For the simulations, the *surface roughness parameter (Ra)* of the walls is considered and it is imposed to the same values measured with the optical microscope: Ra= 16 μm for pad #1 and Ra= 22 μm for pad #2. The surface roughness value has possibly relevant effects on the coolant flow since it could increase the resulting pressure drop. The main reason comes from the interaction between the turbulent regime and the micro-peaks of the

walls surface; therefore this effect is notable only when water is used and turbulent regime occurs. The numerical model is used also to compare the effect of different materials. Solid domain can be made of steel or copper, while fluid domain can work with water or lubricant oil ISOVG68 [31]; such oil is a common industrial choice for the lubricating circuit of the pad. The same oil can be used for the cooling circuit, avoiding any possible contamination issues between lubrication and cooling fluids. Furthermore, the same supply circuit of the lubrication can be used for the coolant. The material properties are obtained from

**Table 5**
Materials thermal properties.

| Material | Density [kg/m³] | Dynamic viscosity [Pa•s] | Specific Heat [J/kg-K] | Thermal conductivity [W/m-K] |
|---|---|---|---|---|
| Steel SS316L | 8030 | - | 502 | 16.27 |
| Copper | 8978 | - | 381 | 387.60 |
| SnSb8Cu4 | 7300 | - | 230 | 45.00 |
| Water | 998 | 0.001 | 4182 | 0.60 |
| Oil ISOVG68 (40 °C) | 878 | 0.04 | 1934 | 0.15 |

the literature and listed in Table 5. The dependence of oil mass density and dynamic viscosity as a function of the temperature are shown in Fig. 11.

### 5.2. Mesh sensitivity analysis

The simulated geometry is composed by two domains, the solid pad structure and the fluid domain, whose meshes are shown in Figs. 12a-b. The total mesh has about $17 * 10^6$ tetrahedral elements with a maximum edge size of 0.5 mm.

Great attention should be given for the generation of the mesh for the lattice domain. Mesh accuracy and shape discretization should be balanced to find a profitable trade-off between reliable results and computation time. In addition, the mesh quality indexes (i.e. maximum aspect ratio) should be checked and minimized to guarantee a good convergence of the solution. Definitively, the setup of these parameters is not an easy task for the mesh of gyroid lattice and great effort has been put to obtain valuable results.

Moreover, the use of $K-\omega\ SST$ model requires the mesh refinement at the walls. A proper *near wall treatment method* is fundamental to solve accurately the boundary layer velocity profile and, consequently, to obtain reliable predictions of the channel pressure drop. Two methods are investigated by considering the *castellation refinement* or the *inflation algorithm* [32] in order to obtain in both cases a maximum $y+$ value lower than the unit at the wall.

The first method thickens the cell density uniformly in space near the outer walls while the second one creates stacked and elongated layers of cells near the walls, a comparison between the two mesh topologies is shown in Figs. 12c-12d.

The castellation refinement reproduces the lattice geometry with great accuracy but it requires a huge computational effort. The resulting mesh is very heavy and it is prone to generate low quality cells and errors depending on little inaccuracies of the starting 3D geometry.

On the counterpart, the inflation algorithm has many advantages since it allows to drastically reduce the number of cells (−80 % of elements), both reducing the computational resources and the time; and it favors the numerical convergence of the solution; whereas it requires a preliminary simplification of the lattice geometry. For example, it is clearly visible the smoothing of the sharp edges in Fig. 12c. This finding is very important and it is proven to have predominant effect on the solution results, as broadly discussed in Section 7. The main reason found is that the relative density of the lattice is slightly increased of (+1; +1.5 %) and the computed counterpressure is highly sensitive to this changing. After many attempts, the *inflation algorithm* is chosen for the mesh, making sure to check again the relative density of the meshed

component. A summary of the main advantages and drawbacks of each technique is shown in Table 6.

Finally, a mesh sensitivity analysis is performed by increasing the number of cells till there are no more changes in the computed variables of interest, i.e. the pressure drop. For the analysis the most critical condition is considered: pad "sheet 35 %", water as coolant at the maximum flow rate for the application (6 L/min). Fig. 13.

### 5.3. Boundary conditions

The simulation is performed in a completely similar way to the previously analysed cylindrical tubes, minor modifications are performed in order to consider the different geometry. For the setup of the simulation, the following boundary conditions (BCs) have been assumed, as shown in Fig. 14. Actually, they are derived from the existing literature for the thermal analysis of lattices and they mimic the experimental conditions. Namely, flow rate and temperature are imposed at the inlet for the coolant, while the outlet is considered isobaric with the atmospheric pressure. The convection with oil is imposed on all the outer walls, that are effectively wetted by the lubricant oil in the real bearing. The biggest simplification is introduced for the *sliding surface* temperature distribution, which is modelled as constant to reduce the model complexity. The value is the mean temperature approximated from Fig. 3c. The stability of the BCs is checked by applying slight changes to prove the stability of the model, finally they are considered reliable for the analysis.

A recap of the applied boundary conditions is reported below:

- Inlet Flow normal velocity: 40 °C
- Outlet Atmospheric pressure
- Sliding surface Imposed temperature: 60 °C
- Other walls Convection with oil at 50 °C, $h = 50 W/m^2 \bullet K$

### 5.4. CFD results analysis

The results of the CFD analysis are listed in Table 7 for a fluid flow rate of 6 L/min, where the thermo-fluid dynamic properties are quantified in terms of pressure drop in the channel and heat exchange, between the solid part and the coolant. The baseline solution and gyroid "sheet 35 %" lattice are compared, for different fluids (water and oil ISOVG68) and solid materials (SS316L steel and copper).

First of all, it is important to compare the cooling power values with respect the estimation of the heat production, due to frictional losses. From the TEHD model of the baseline solution, power loss is about 600 W on the bottom pad, so gyroid lattice can extract a significant
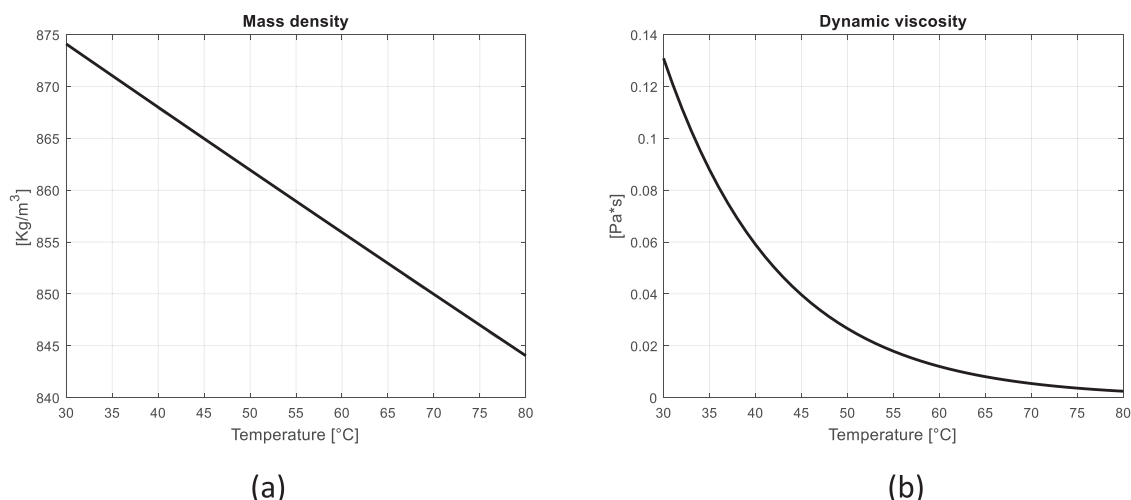


**Fig. 11.** Oil ISOVG68 properties as function of temperature: (a) mass density, (b) dynamic viscosity.
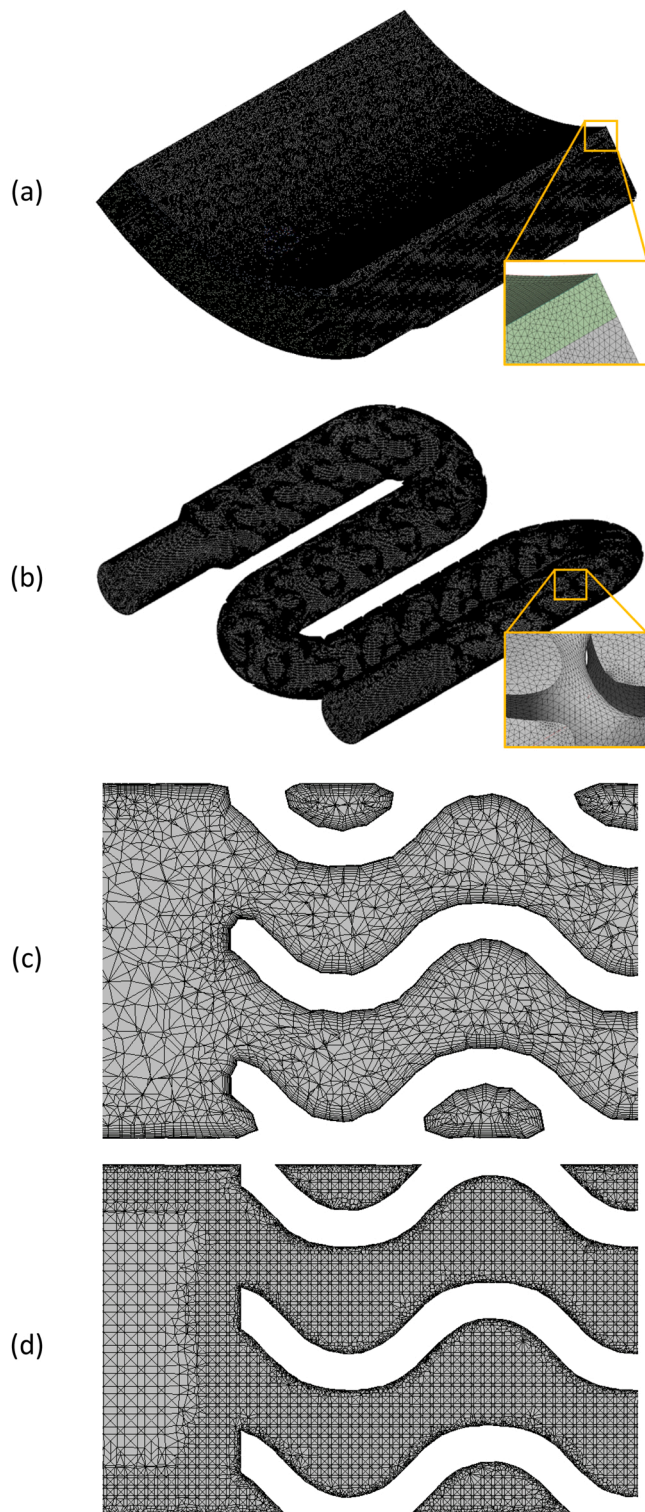
**Fig. 12.** CFD space discretization: a) mesh of solid domain; (b) mesh of fluid domain; (c) inflation refinement at wall; (d) castellation refinement at wall.

quantity of the generated heat. When water and copper are used, the cooling power seems to be higher than the heat production rate: actually, this is a consequence of the fix-temperature boundary condition assumed for the sliding surface, useful for the following comparative analysis but not accurate in representing the real case.

When oil is used as coolant, no significant advantages can be highlighted for the steel pad, probably because the excessive coolant viscosity limits the beneficial effect of vorticity imposed by the lattice. For

**Table 6**
Pros and cons comparison of near wall treatment methods.

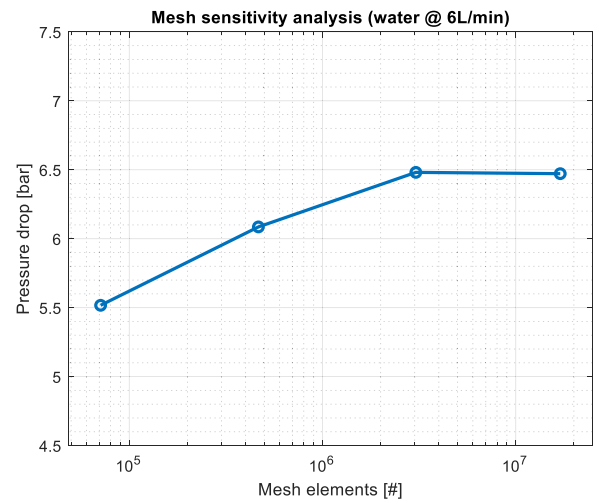|  | | Castellation algorithm | | Inflation algorithm |
|---|---|---|---|---|
| Computational effects | ✘ | Resources onerous | ✔ | Coarser mesh |
| | ✘ | Time expensive | ✔ | Faster computation |
| | ✘ | Prone to errors | ✔ | Better convergence |
| Geometrical effects | ✔ | Wall y+ < 1 | ✔ | Wall y+ < 1 |
| | ✔ | Accurate reconstruction | ✘ | RD error (1-1.5%) |
| | ✘ | Low cell quality | ✔ | Good cell quality |



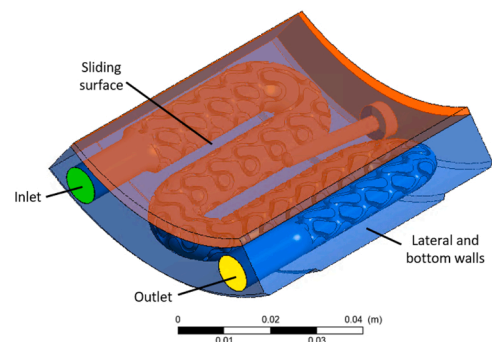**Fig. 13.** Mesh sensitivity analysis on cell number for pad "sheet 35 %".



**Fig. 14.** Boundary conditions for CFD simulation setup.

**Table 7**
CFD material analysis for fluid flow rate of 6 L/min.

| Internal Layout | Fluid material | Solid material | Pressure drop [bar] | Exchanged heat [W] |
|---|---|---|---|---|
| 6-channels | Oil ISOVG68 | SS316L | 0.983 | 160 |
| | Water | SS316L | 0.121 | 248 |
| | Water | Copper | 0.121 | 877 |
| Sheet 35% | Oil ISOVG68 | SS316L | 10.071 | 212 |
| | Water | SS316L | 2.884 | 373 |
| | Water | Copper | 2.884 | 1120 |

the "sheet 35 %" lattice, a rather high pressure drop of approximately 10 bar is obtained. Conversely, the improvements are notable when using water and gyroid lattice increases the heat exchange considerably up to + 50.4 %, with respect to the baseline 6-channels pad. Similarly to tubes case, the OEF for pad circuit is calculated with respect to an M-

shaped channel with circular cross section (internal diameter 9 mm) here not reported for brevity. By comparing the OEF values for tubes and for pad, similar values can be found for "sheet 35 %" lattice in case of steel. The computed OEF when oil is used as coolant is 0.11 and with water is 0.54. This is an important confirmation of the simplification hypothesis previously performed.

Finally, the use of copper is a promising solution and it would increase the performances of gyroid lattice when coupled with water as coolant. It is here proposed only referring to the thermal properties, while the mechanical properties are preliminary checked and they are compatible with the application. By using copper, pressure drop remains the same while the exchanged heat increases by + 200 % both for 6-channels and gyroid lattice compared to the respective geometries made of steel. Further studies and tests are required with a copper alloy suitable for BMD process.

Moreover, it is interesting to consider the flowing regime by using the *Turbulent Intensity (TI)* as a convenient indicator [33]; usually it ranges between 0 % (laminar flow) and 30 % (fully turbulent flow). Reynolds number is not used, because it is difficult to define the reference dimensions for a complex structure such as gyroid lattice. In the simulations, a typical value of TI= 5 % is imposed at fluid inlet (common choice to mimic the fluid flowing in a straight pipe) and the same parameter is checked at lattice outlet. From the results, oil reaches a TI≈ 0 % in the cooling circuit, therefore flow regime is purely laminar and heat convection is controlled by the large eddies of the coolant, imposed by the lattice; while water reaches the turbulent regime (TI≈20 %), which guarantees a remarkable increasing of the effective heat transfer rate.

The pressure fields for the baseline and "sheet 35 %" pads are shown in Fig. 15, when oil is used as coolant, whereas the temperature distributions are shown in Fig. 16 for the water case. The sections are chosen to be the best representative for the corresponding shown variable.

It is also notable to consider the effect of flow rate on the two geometries. This comparison is the most effective, because the gyroid lattice base concept is to induce the fluid turbulence. The pressure drop $\Delta P$ and the heat exchange $Q$ as a function of the coolant flow rate are shown in Fig. 17 and Fig. 18 respectively, for the baseline 6-channels pad and for "sheet 35 %" layouts, both in the case of oil and water as coolant. The maximum flow rate for the application is considered to be 6 L/min and a flow rate of 12 L/min is computed only to compare the trend lines. Looking at the pressure curves, the behavior is similar for the two coolants, but considerably higher pressures values are required for the oil case, just depending on its higher viscosity than the water. However, the exchanged heat trend is different for the two coolants. In

the case of oil the flow regime is laminar, both in 6-channels and gyroid layout, so the curve shape is similar and simply shifted upward, due to the higher wetted surface of gyroid channel. Conversely, when the water is considered, the flow regime becomes turbulent in the gyroid channel and the heat exchanged can be relevantly increased. Therefore, gyroid heat exchange performances are clearly favorable, when turbulence occurs and the advantage between the two geometries increases for higher coolant flow rate.

## 6. Experimental flushing test

### 6.1. Experimental setup

The experimental campaign is carried out to validate the pressure drop values of the numerical model with oil ISOVG68 and water. The experimental setup is mainly composed of two subassemblies, the hydraulic system and the flushing circuit. The external hydraulic system has been used to provide pumping pressure and to keep the oil temperature at 40 ± 1 °C by means of a temperature controller. The oil viscosity (and the directly related pressure drop) is very sensitive to the temperature. The oil inlet temperature value is chosen as a reference, because it is a significant operation parameter for the cooled pad.

When water is used, the pumping arrangement is substituted by a pressurized circuit with water at ambient temperature (17 °C); note that temperature control is no more significant in this case.

The flushing circuit is shown in Fig. 19a, where the coolant flows from the left to the right passing through a temperature probe and reaching a crossroad regulated by two manual valves. The lower branch is used for the recirculation of the oil during the start-up procedure, allowing the thermal regime to be achieved, before starting with measurements, while it is not used for water. Right branch contains a pressure probe immediately before the pad sample, while the lattice outlet port can be considered isobaric with the ambient pressure. The fluid flow rate is adjusted with a regulating valve on the hydraulic system and then checked by weighting out the coolant flowed in a certain time interval with a scale.

The measuring set-up is shown in Fig. 19b, with the insulated pad on the left and a becker for fluid weighting on the digital scale. The pad is insulated with a thermal protection in polystyrene to keep it at desired temperature. The nominal flow rate is ranged from 1 L/min to 6 L/min, by acting on the regulating valve of the hydraulic system, but flow rates higher than 3 L/min are not reachable for the oil, because they require an excessive hydraulic head for the pump; a similar issue occurs also for the water. Since connecting tubes have quite small diameter, their
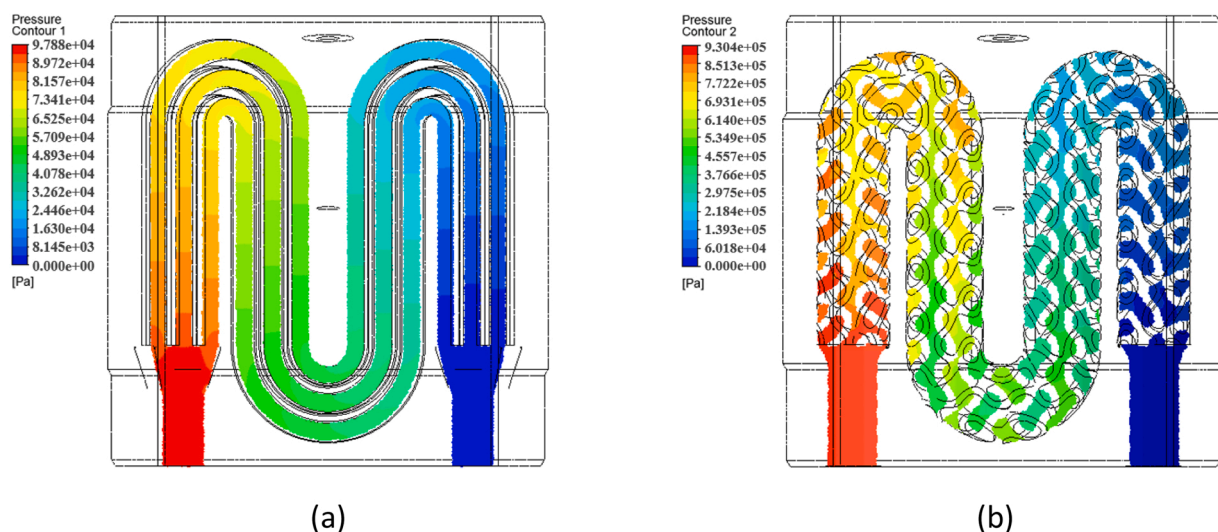


(a)                    (b)

**Fig. 15.** CFD analysis, comparison of pressure field on meridian cross section, oil ISOVG68, 6 L/min: (a) baseline 6-channels, (b) "sheet 35 %" lattice.
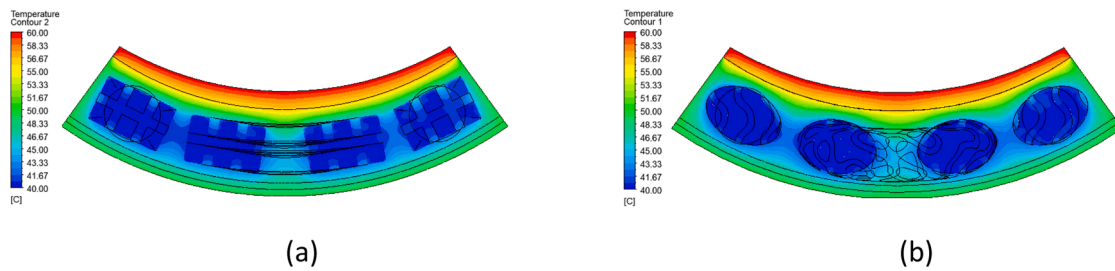
**Fig. 16.** CFD analysis, comparisons of temperature distribution on transversal cross section, water, 6 L/min: (a) baseline 6-channels, (b) "sheet 35 %" lattice.
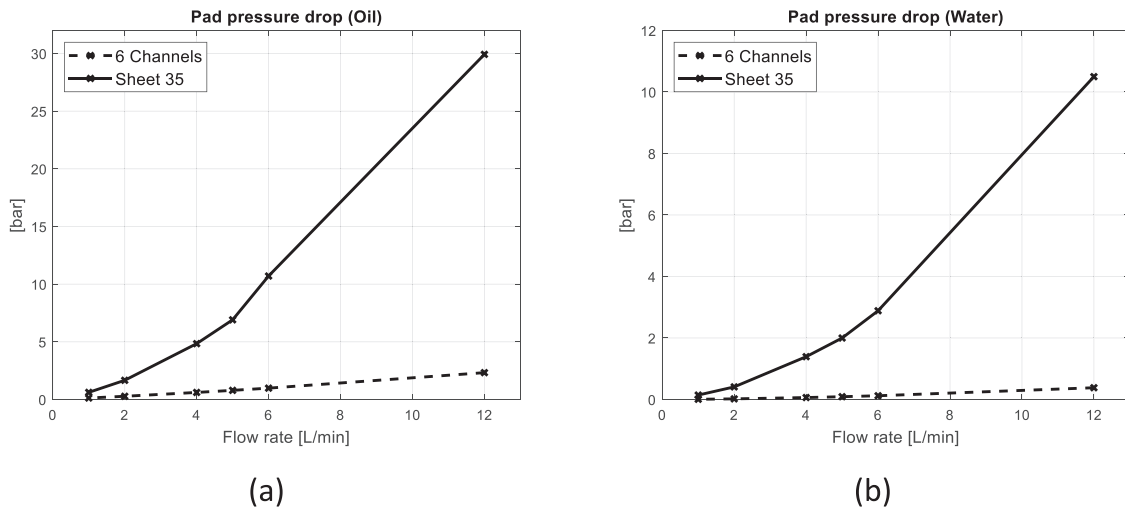


**Fig. 17.** CFD pressure drop comparison as a function of flow rate for the two geometries by using oil (a) and water (b) as coolant.
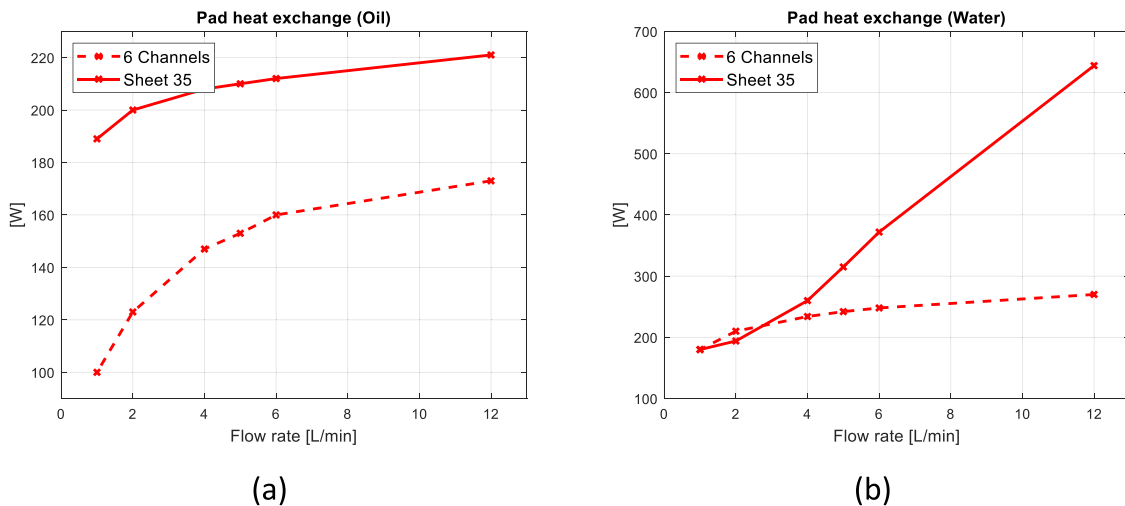


**Fig. 18.** CFD heat exchange comparison as a function of flow rate for the two geometries, by using oil (a) and water (b) as coolant.

pressure drop can be significant, so they are flushed separately, by connecting them in series, to consider their pressure drop contribution.

Since flow rate is not closed loop controlled, operating conditions are checked for each measurement: the pressure and the temperature are measured by sensors, while the flow rate is calculated and adjusted. The measures are performed on the two printed pads, both with oil and water. They are repeated five times for robustness and uncertainty analysis is performed. The average error on flow rate is ± 0.3 %, while sensitivity for pressure is ± 2mbar and for temperature is ± 1 °C. All the measuring uncertainties are considered acceptable for the characterization of the pad.

### 6.2. Experimental results analysis

The resulting resistance curve (pressure versus flow rate) is obtained with a 2-order polynomial regression. For the mathematical model, zero-order term is imposed null to reflect physics of the problem, the confidence and the prediction intervals are plotted with a confidence level of 95 %. The measures figure out a high repeatability, as proved by the high values of the computed Correlation coefficient (*R-Sq*), around 99 %; then no disturbance effects have arisen when experiments are performed. During the oil flushing, the temperature fluctuations have been the most critical variable to be controlled because of the external
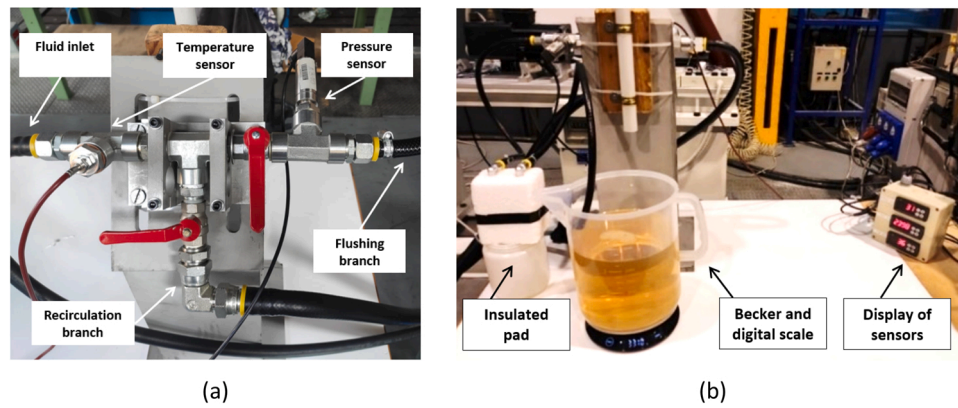
**Fig. 19.** Flushing hydraulic circuit (a) and measuring set up (b).

environmental disturbances, nevertheless a fine tuning of the set-up was sufficient to keep the oil temperature constant, obtaining low influences on the measures. The resulting pressure curves for the pad #1 are reported in Fig. 20, for both oil and water, while results for pad #2 are shown in Fig. 21. By looking at the data, it is noteworthy to consider that pad #2 requires a higher counterpressure (approximately +23.6 % with oil and +14.7 % with water) than pad #1 at the same operating conditions. Since the nominal geometry is equal, the differences can be addressed only to the change in the layering orientation, and so, to the surface roughness and to the printing accuracy of the internal channels.

Finally, experimental flushing has been performed also on 6-channels pad. Even though this prototype comes from some previous research activities, there were no reliable measures of its experimental counterpressure. These quantities are interesting to validate the numerical model of the baseline solution, so it has been flushed in the same manner of the other pads. The resulting pressure curves are shown in Fig. 22.

## 7. Comparison between CFD simulation and experimental results

The experimental results of pressure data are used to properly tune the numerical model, by considering the flushing of the two pads both with oil and water as coolant. In order to quantify the differences in an accurate way, interpolating polynomials are calculated from raw data and then used to estimate the pressure curves at nominal flow rates from 1 L/min to 3 L/min. The pressure drop related to the connecting tubes is

subtracted and the comparison between numerical and experimental pressure curves is shown in Fig. 23. By looking at the results for the gyroid pad, the numerical model with the nominal geometry (sheet RD=35 %) relevantly underestimates the experimental values. Moreover, the pressure error increases with flow rate in both cases. The difference between pad #1 and pad #2 is evident and it related to the lower printing accuracy measured on pad #2, as already mentioned in Section 6.2. When looking at 6-channels pad, the pressure error is less significant and it is almost constant with respect to flow rate, probably because of the easier shape of the channels and the different AM process used (Selective Laser Melting). The comparison between the numerical and the experimental results clearly show a lack in the numerical model that is strictly related to the manufacturing technique of the prototypes.

As discussed by Hartsfield et al. in [34], the estimation of flow characteristics of AM parts, like the pressure drop, is still cumbersome. The numerical model should take into account for local and generalized printing defects and the layering effect on the surface roughness, which are difficult to estimate a priori because they depend on the geometry and the printing setup parameters. The authors here propose a preliminary investigation of this topic, by performing a qualitative geometrical check on the printed geometry. A reasonable explanation of the pressure differences depends on three main aspects:

- Macroscopic printing errors;
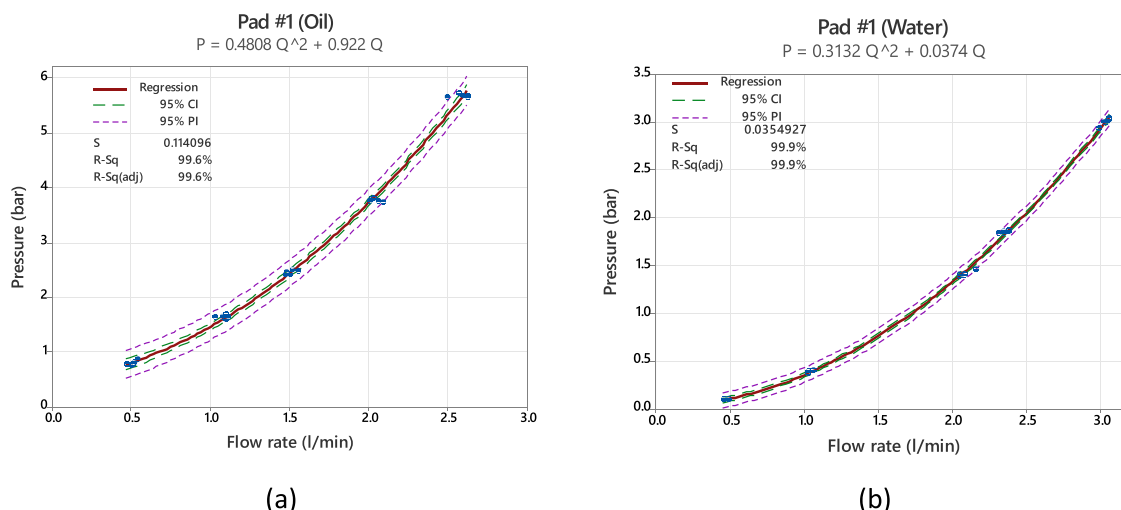- Actual relative density;
- Wall roughness;



**Fig. 20.** Experimental pressure curve for pad #1 in oil (a) and water (b) measured with tubes.
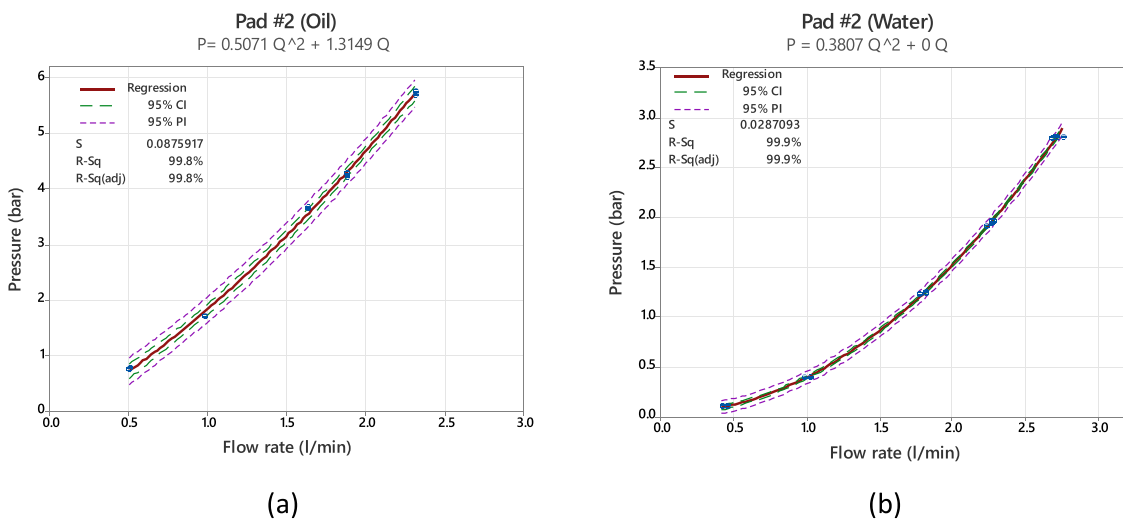
**Fig. 21.** Experimental pressure curve for pad #2 in oil (a) and water (b) measured with tubes.
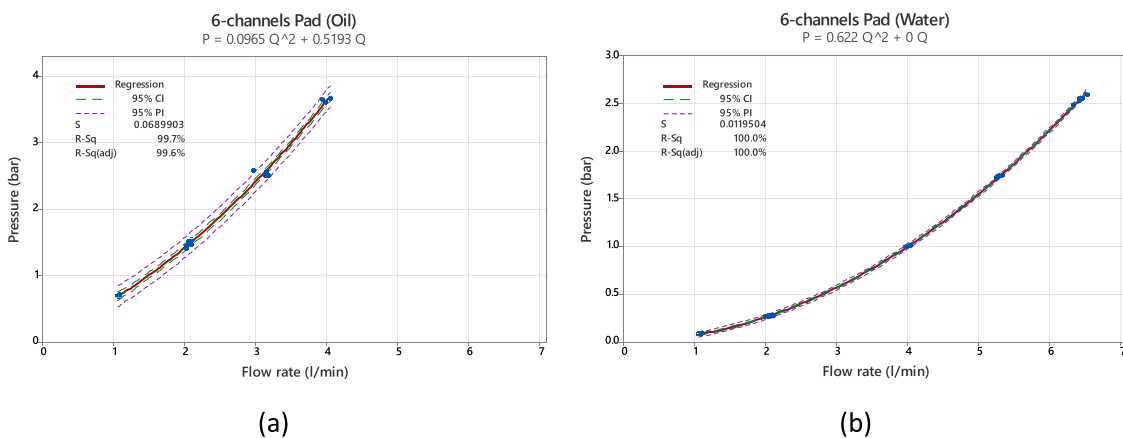


**Fig. 22.** Experimental pressure curve for 6-channels pad in oil (a) and water (b) measured with tubes.
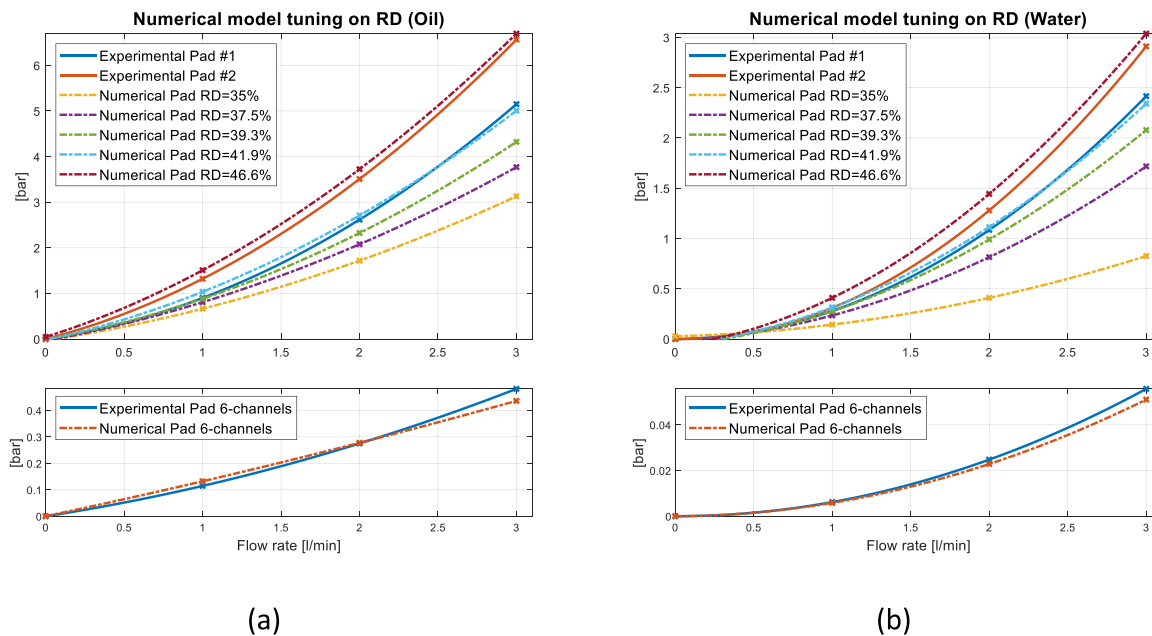


**Fig. 23.** Pressure curves for pad #1, pad #2 and 6-channels; tuning of CFD model for Relative density in oil (a) and water (b).

The first aspect can be caused, for example, by incorrect nozzle deposition in green parts or anisotropic shrinkage, which give rise to localized pressure losses. The internal geometry of pad #2 is inspected by means of *Computed tomography* (X-Ray CT) scans. The results are attached to this paper as MP4 videos in the supplementary material. Some localized dross formation and filament detachment are noticed, in particular near overhang regions, as shown in Fig. 24. These errors are interesting but difficult to be modelled in the numerical analysis. Unfortunately, it is not possible to perform reliable calculations to measure the printed relative density because of an insufficient scanning accuracy. Anyway, it is certain that the presence of diffused printing defects affects in a negative way the fluid dynamic performances of the cooling channel. This can be a reasonable justification for the measured pressure differences, both for the oil and water case and it will be discussed in this section.

Finally, the surface roughness parameter has to be considered. Even though this indicator is very sensitive to the layering choice and so to the printing accuracy, actually it is not convenient for a process of parametrical tuning. First of all, the measured roughness values are not useful for the CFD codes because they use a sand-grain roughness model. Unfortunately this is not suitable for AM parts because it neglects the important effects of oriented layering and directional roughness which are dominant for AM parts. Moreover, the wall roughness affects the counter pressure value only in turbulent regime (water coolant for the case study) but not in laminar regime when oil is used, as discussed in Section 5.1. Thereby, the roughness parameter is not effective for the tuning process.

As a consequence of the mentioned remarks, the tuning process of the CFD model is performed on the Relative Density (*RD*) parameter in order to reproduce the experimental pressure curves both in oil and water cases. As already mentioned in Section 5.2, the pressure drops values estimated by the numerical model are highly sensitive to the relative density of the sheet lattice, this important outcome is exploited to correctly tune the numerical model.

A sensitivity analysis is performed by repeating the numerical simulations; all the boundary conditions and the setup procedure are kept the same and only the relative density of the lattice is increased step by step from 35 % to approximately 45 % (Fig. 23). For this activity it is convenient to express the average increase of the pressure curve as percentage with respect to the numerical pressure curve calculated for pad with "sheet 35″" lattice. For each simulation two values of density are given, before and after the meshing approximation for the Inflation algorithm, as discussed in the previous sections. This procedure assures a higher accuracy for the results because it takes into account the geometrical simplification given by the mesh. The computed pressure data both for oil and water are shown in Fig. 25 and reported in a tabular way in Table 8.
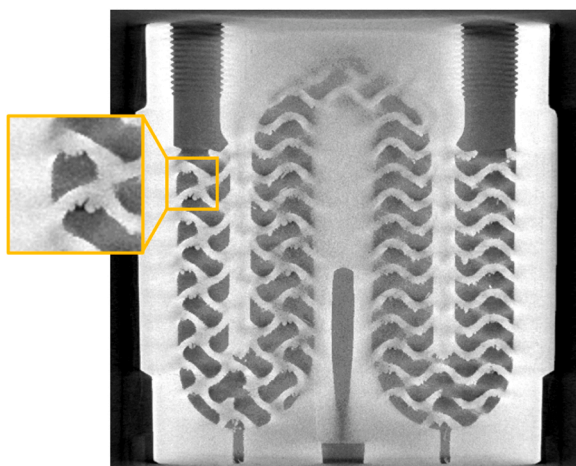
The graph shows the percentual increase of pressure by changing the relative density for the numerical model and the respective regression 2 order polynomial equations are calculated. The experimental regression lines for the correlation between the pressure increase and the relative density are reported in Table 8 and they become important for the design of the manufactured component. Both oil and water case are represented, moreover the experimental pressure values for pads #1 and #2 are reported as yellow markers of different shape. By inverting the computed equations and by applying them to the experimental pads, the required relative densities can be estimated. Pad #1 can be modelled with an equivalent numerical model with relative density around 42 % while pad #2 around 46 %. Please consider that these equivalent values of relative densities take into account all the inaccuracies of the manufacturing step and they may not correspond to the geometrical definition. This solution finds good agreement both for the oil and the water cases and the main results are summarized in Table 9.

About the validity limits of the empirical equations is north worthy to state that they are suitable only for the current case of study, nevertheless the important aspect is the strong sensitivity of the pressure drop with respect to the relative density and this procedure can be easily reproduced for any other component. The most relevant outcome of the tuning process is that the printed lattices are featured by localized and diffused printing defects, which affects relevantly the counter pressure and they should be taken into account for the design of the component.

## 8. Conclusions

Bioinspired gyroid lattice is confirmed to be an effective solution for light-weighting of structural components and enhanced heat exchange. Static mechanical analysis and fluid dynamics properties have been deeply investigated in this paper by means of numerical simulations and experimental tests, to better understand the most suitable design set up for cooled pad in TPJB.

The application on TPJB has great opportunities of improvements: advanced internal cooling can reduce sliding surface temperature with beneficial effects on the bearing behavior. In particular, for gyroid lattice, heat exchange can be increased at least of + 50 % with respect to the baseline solution. This investigation contributes to the worldwide trend to increase efficiency and performances of machines in engineering. More loaded pads, with the limit given only by the liner mechanical characteristics, allow downsizing of oil film bearings, reducing the quantity of oil needed for lubrication and pushing this widely used technology to a more environmentally friendly level, especially if water
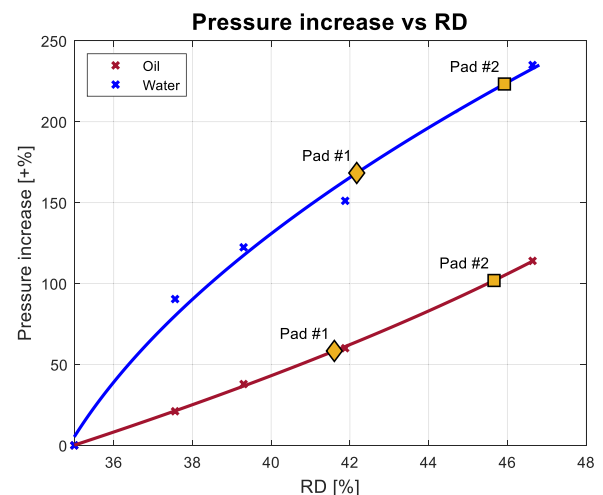


**Fig. 24.** X-Ray CT scan of the printed pad #2, meridian section.



**Fig. 25.** Sensitivity analysis of pressure increase as a function of relative density (RD), numerical results.

**Table 8**
Tabular data of pressure increase as a function of relative density (RD).

| Relative Density (before meshing) | Relative Density (after meshing) | Pressure increase (oil) | Pressure increase (water) |
|---|---|---|---|
| 35 % | 35.0 % | +0 % | +0 % |
| 35 % | 37.6 % | +21 % | +90 % |
| 37 % | 39.3 % | +38 % | +122 % |
| 40 % | 41.9 % | +60 % | +151 % |
| 45 % | 46.6 % | +143 % | +226 % |

| Regression functions Validity range: $RD \in [35\%; 47\%]$ | $\Delta p_{oil} = 0.1816 RD^2 - 5.09 RD - 44.04$ |
|---|---|
| | $\Delta p_{water} = -0.8206 RD^2 + 86.13 RD - 2001$ |

**Table 9**
Equivalent relative densities computed for the model tuning on pads.

| | Coolant type | Pressure increase (oil) | Equivalent relative density |
|---|---|---|---|
| Pad #1 | oil | +58 % | 41.6 % |
| | water | +168 % | 42.2 % |
| Pad #2 | oil | +102 % | 45.7 % |
| | water | +223 % | 45.9 % |

is used for the internal cooling.

For further developments, a Thermo-Elastic-Hydro-Dynamic model of the bearing could be implemented so that temperature distributions on pad surfaces are directly calculated at each iteration, leading to a more representative and reliable model of the bearing. Unfortunately, gyroid geometry is quite complicated and an efficient mesh solution becomes fundamental to avoid a too large computational effort in the CFD analysis.

The manufacturing of functional prototypes by means of Bound Metal Deposition is the key outcome of this research activity. Manufacturing setup have been tuned carefully to counterbalance geometrical and dimensional defects. Moreover, the absence of excess metal powder inside the channels and easy printing of copper are relevant advantages of this technology.

Finally, comparisons between numerical and experimental data are useful to catch printing differences with the nominal geometry and to quantify the accuracy of the proposed numerical model.

## Statement of originality

I confirm that this paper is original and it has not been published previously and it is not under consideration elsewhere.

## Declaration of Competing Interest

The authors declare that they have no known competing financial interests or personal relationships that could have appeared to influence the work reported in this paper.

## Data availability

Data will be made available on request.

## Acknowledgements

## Appendix A. Supporting information

Supplementary data associated with this article can be found in the online version at doi:10.1016/j.triboint.2023.108448.

## References

[1] Stephen W, Giddings C, Lee S. Characterization of hydrodynamic lift forces by field-flow fractionation. inertial and near-wall lift forces. Chem Eng Commun 1994; 130:143–66.
[2] Kim S, Shin D, Palazzolo AB. A review of journal bearing induced nonlinear rotordynamic vibrations. J Tribol 2021:143.
[3] Fillon M. Thermal and deformation effects on tilting-pad thrust and journal bearing performance;, 2005.
[4] Dong Q, Yin Z, Li H, Gao G, Zhong N, Chen Y. Simulation and experimental verification of fatigue strength evaluation of journal bearing bush. Eng Fail Anal 2020;109:104275. https://doi.org/10.1016/j.engfailanal.2019.104275.
[5] Yang S, Kim C, Lee W. Prevention of fluttering fatigue damage in a tilting pad journal bearing. Tribol Int 2009;42:816–22.
[6] Mehdi SM, Jeong SY, Kim TH. Influence of recess dimensions and jacking oil flow rate on the performance of tilting pad journal bearings with jacking oil mechanism. Tribol Trans 2022;0:1–16.
[7] Cerda Varela A, Ferreira Santos I. Dynamic coefficients of a tilting pad with active lubrication: comparison between theoretical and experimental results. J Tribol 2015:137.
[8] Hagemann T, Schwarze H. Theoretical and experimental analyses of directly lubricated tilting-pad journal bearings with leading edge groove. J Eng Gas Turbines Power 2018:141.
[9] Abdollahi B, San Andrés L. Improved estimation of bearing pads' inlet temperature: a model for lubricant mixing at oil feed ports and validation against test data. J Tribol 2018:141.
[10] Croné P, Almqvist A, Larsson R. Thermal turbulent flow in leading edge grooved and conventional tilting pad journal bearing segments—a comparative study. Lubricants 2018;6:97.
[11] Varela AC, Santos IF. Component level study of an actively lubricated LEG tilting pad bearing: theory and experiment. Tribol Int 2018;120:115–26.
[12] Schüler E, Berner O. Improvement of tilting-pad journal bearing operating characteristics by application of Eddy grooves. Lubricants 2021;9:18.
[13] Yang J, Palazzolo A. Power loss reduction for tilt pad journal bearings utilizing pad pockets and steps. Tribol Int 2021.
[14] Najar FA, Harmain GA. Novel approach towards thrust bearing pad cooling. Am Soc Mech Eng Digit Collect 2015.
[15] Najar F, Harmain G. Performance characteristics in hydrodynamic water cooled thrust bearings. J Tribol 2016;10:28–47.
[16] Chatterton S, Pennacchi P, Vania A, Dang PV. Cooled pads for tilting-pad journal bearings. Lubricants 2019;7:92.
[17] Suh J, Palazzolo A. Three-dimensional dynamic model of TEHD tilting-pad journal bearing—part i: theoretical modeling. J Tribol 2015;137.
[18] Kaur I, Singh P. State-of-the-art in heat exchanger additive manufacturing. Int J Heat Mass Transf 2021;178:121600.
[19] Li W, Yu G, Yu Z. Bioinspired heat exchangers based on triply periodic minimal surfaces for supercritical $CO_2$ cycles. Appl Therm Eng 2020;179:115686.
[20] Luo J-W, Chen L, Min T. Macroscopic transport properties of Gyroid structures based on pore-scale studies: permeability, diffusivity and thermal conductivity. Int J Heat Mass Transf 2020;146:118837.
[21] Peng H, Gao F, Hu W. Design, modelling and characterization of Triply Periodic Minimal Surface heat exchangers with Additive Manufacturing; 2019.
[22] Michielsen K, Stavenga D g. Gyroid cuticular structures in butterfly wing scales: biological photonic crystals. J R Soc Interface 2008;5:85–94.
[23] Koneri R, Mulye S, Ananthakrishna K. Additive manufacturing of lattice structures for heat transfer enhancement in pipe flow. Ind. 40 adv. manuf. Singapore: Springer; 2021. p. 233–46.
[24] Zhang L, Feih S, Daynes S. Energy absorption characteristics of metallic triply periodic minimal surface sheet structures under compressive loading. Addit Manuf 2018;23:505–15.
[25] Al-Ketan O, Rezgui R, Rowshan R. Microarchitected stretching-dominated mechanical metamaterials with minimal surface topologies. Adv Eng Mater 2018; 20:1800029.
[26] Parenti P, Puccio D, Colosimo BM. A new solution for assessing the printability of 17-4 PH gyroids produced via extrusion-based metal AM. J Manuf Process 2022;74: 557–72.
[27] 3D printing: desktop metal dimensional accuracy & surface finish. comput aided technol LLC; 2022. Available from: 〈https://www.cati.com/blog/2019/05/desktop-metal-dimensional-accuracy-surface-finish/〉.
[28] Dang PV, Chatterton S, Pennacchi P. The effect of the pivot stiffness on the performances of five-pad tilting pad bearings. Lubricants 2019;7:61. https://doi.org/10.3390/lubricants7070061.
[29] Chatterton S, Pennacchi P, Dang PV, Vania A. A test rig for evaluating tilting-pad journal bearing characteristics. Mech Mach Sci 2015;21:921–30.
[30] Khaderi SN, Deshpande VS, Fleck NA. The stiffness and strength of the gyroid lattice. Int J Solids Struct 2014;51:3866–77.
[31] Petronas arbor hydraulic 68 ISO VG 68. Petronas Lubr Cat; 2021. Available from: 〈https://www.pli-petronas.com/it-it/agricoltura-e-macchine-movimento-terra/prodotto/petronas-arbor-hydraulic-68-iso-vg-68〉.

[32] Ferziger JH, Perić M. Computational methods for fluid dynamics. Berlin, Heidelberg: Springer; 2002.

[33] Marusic I, Kunkel GJ. Streamwise turbulence intensity formulation for flat-plate boundary layers. Phys Fluids 2003;15:2461–4.

[34] Hartsfield CR, Shelton TE, Cobb GR, Kemnitz RA, Weber J. Understanding flow characteristics in metal additive manufacturing. J Aerosp Eng 2021;34:04021082.